From strings to coils: Rotational dynamics of DNA-linked colloidal chains

Steve Kuei, Burke Garza, and Sibani Lisa Biswal
Department of Chemical and Biomolecular Engineering, Rice University, Houston, Texas 77005, USA
(Received 1 February 2017; published 16 October 2017)

We investigate the dynamical behavior of deformable filaments experimentally using a tunable model system consisting of linked paramagnetic colloidal particles, where the persistence length l_p, the contour length l_c, and the strength and frequency of the external driving force are controlled. We find that upon forcing by an external magnetic field, a variety of structural and conformational regimes exist. Depending on the competition of forces and torques on the chain, we see classic rigid rotator behavior, as well as dynamically rich wagging, coiling, and folding behavior. Through a combination of experiments, computational models, and theoretical calculations, we are able to observe, classify, and predict these dynamics as a function of the dimensionless Mason and magnetoelastic numbers.

DOI: 10.1103/PhysRevFluids.2.104102

I. INTRODUCTION

The response of stiff and semiflexible filaments in fluids to driving forces is the basis for naturally occurring and practically relevant phenomena, from flagellar motion [1–3] and microfluidic fluid manipulation [4,5] to gelation and bulk polymer properties [6,7]. Starting from the theoretical orbits derived by Jeffery for rigid filaments [8], the dynamics of rigid and flexible non-Brownian fibers [9,10] and Brownian filaments like DNA and actin [11–13] have been systematically investigated. Lang *et al.* point out that there is currently a wealth of knowledge in both rigid and highly flexible polymer regimes, with good agreement between experimental results and scaling laws. However, in the intermediate semiflexible polymer regime, where practically useful fibers such as actin, carbon nanotubes, and cilia reside, many questions remain unanswered, from subperiod dynamics and their effects on fluid propulsion to the existence and significance of self-entanglement, entanglement, and other topological effects on bulk properties.

Despite revolutionary experimental work on fibers such as actin and microtubules, the limited resolution makes it difficult to study subperiod and subchain dynamics. Many have turned to computational models to supplement their studies, which has yielded a wealth of information [14–18]; however, these are still limited by the unfavorable scaling of complex hydrodynamic interactions.

Here we utilize colloidal particle chains as an experimental model with which to probe semiflexible chain dynamics, as this model system has the tunability, control, and resolution of computational models, while avoiding the size-dependent scaling of numerical force calculations. Previously, others have shown that magnetically controlled particle chains can be actuated by externally controlled magnetic fields. When a rotating magnetic field is used, the particle chains can rotate synchronously or asynchronously with the external field [19], with the latter often leading to fragmentation in unlinked chains [20] and collapsed hairpins in linked chains [19,21]. These dynamics have begun to be harnessed for use in swimmers [1], biomimetic cilia systems [21], and cargo capture and transport [22], among others.

We seek to demonstrate the application of this colloidal model to the study of semiflexible filaments under a rotational force field. It has been shown previously in shear fields that even in the case where rigid objects yield predictable closed orbits [23], the addition of flexibility yields complicated dynamics such as orbit drift, irreversible deformations, and coil-stretch dynamics [11,12,14,24,25].

In a simpler rotational force field, filament flexibility also generates nonsteady motion, such as stick-slip dynamics [21,22], even in relatively short and stiff chains. Here we explore the dynamics under a steadily rotating magnetic field, as we push into longer, semiflexible filaments, and observe

everything from steady dynamics to persisting deformations to unsteady but reversible deformations, even if filament persistence length is held constant. Through numerical simulation and analytical predictions, we look to predict the dynamics and confirm our understanding of the forces responsible for our experimental results.

II. METHODS

A. Colloidal particle chains

The colloidal spheres used in this work have ferrite grains embedded in a polystyrene matrix, giving it paramagnetic properties; they are also surface functionalized with streptavidin, providing a simple linking chemistry. They are purchased from Life Technologies (Dynabeads® MyOne Streptavidin C1, 10 mg/mL), have a diameter of 1.07 μm, and have a magnetic susceptibility $\chi = 1.377$. They are washed three times with distilled water before being resuspended to 0.01 wt. % in deionized water [26].

Chains are synthesized in a 40-μL flow cell (20 mm $\times$ 20 mm $\times$ 100 μm) between two coverslips (Ted Pella, microscope glass coverslips, # 1.5), using double-stick tape as a spacer, and epoxy (Hardman® Double/Bubble) to seal against evaporation. The coverslips are cleaned using oxygen plasma and suspended in a concentrated potassium hydroxide solution for 30 min to prevent beads from adhering to the glass. The linking solution consists of paramagnetic beads, biotinylated DNA, and a phosphate buffer at final concentrations of 0.0425 wt. %, 5 nM, and 10 nM, respectively, in distilled water. The colloidal spheres are more dense than water and therefore sediment to the bottom plane of the flow cell. Upon applying a constant magnetic field, the beads self-arrange into linear structures to minimize their energy. When held under this field, the beads are in close enough proximity for the DNA linkers to chemically bind neighboring beads together.

The linker length, the strength of the constant linking field, the time held under this field, and the temperature of the chamber can be varied to tune both the length N and persistence length l_p of the final chains; full details can be found in [27]. Here the linking DNA used is a 2000-base-pair segment of λ-DNA (New England Biolabs, Ipswich MA) biotinylated on the 5' ends, the constant linking field is 146 G, and the flow cell is held at 60 °C for 45–90 min (for lower to higher N). Unlike the previous work, flow cells are only partially sealed with epoxy and placed in a humidity chamber during the linking period to minimize evaporation. At the end of the linking time, approximately 5 μL of biotin (0.6 μM) is flowed into the cell to replace the lost volume, capping any unbound streptavidin sites and quenching the linking reaction. Otherwise, chains in nonlinear conformations can permanently bind to themselves during the course of our experiments, impacting the dynamics.

Chains are imaged on an Olympus IX71 inverted microscope (Olympus, Tokyo) using a 100× oil immersion objective and captured using an attached ORCA-ER digital camera (Hamamatsu Corp., Japan) and the program SIMPLEPCI. Image conversion and analysis is conducted using IMAGEJ and MATLAB, using a modified particle tracking package [28].

Our resulting chains have lengths from $N = 2$ to $N > 200$, although we study chains from $N = 5$ to $N = 70$ in this work, due to difficulties in imaging the longer chains. The chains closely follow a discrete wormlike chain approximation, justifying their use as a semiflexible chain model; we find that there is an average spacing of 0.3 μm between each bead in the chain such that $l_0 \approx 1.3d$ and the persistence length is measured to be $l_p \approx 1.3$ mm. These measured values are used in our computational model as well.

To actuate our chains, magnetic fields are applied using two pairs of orthogonally placed solenoids. Using a power supply (Hewlett-Packard 8904A) to run sinusoidal currents through each pair of solenoid coils, we generate the magnetic fields $H_x = H_0 \sin(2\pi f t)$ and $H_y = H_0 \sin(2\pi f t + \pi/2)$, which rotate in plane with frequency f and magnitude H_0.

B. Bead-spring model

The resulting experimental system strongly resembles a bead-spring system of N spheres of radius a, separated by $N - 1$ springs of equilibrium length l_0, resulting in a chain of length

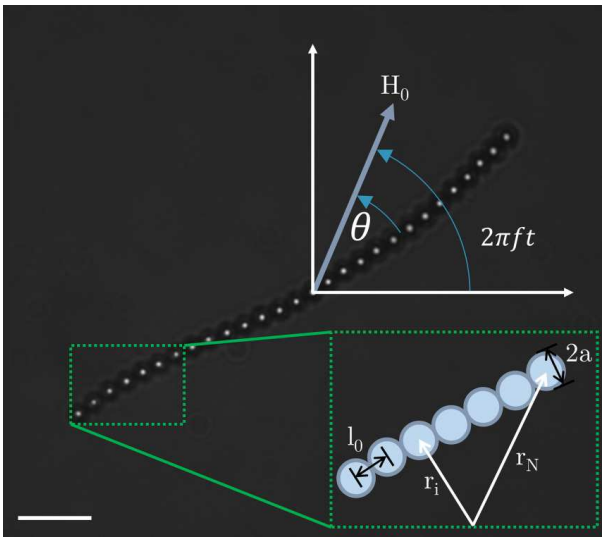

FIG. 1. Colloidal particle chain aligned at a phase lag θ from the external magnetic field $\mathbf{H}_{\text{ext}} = \mathbf{H}_x + \mathbf{H}_y$. This can be described by a bead-spring model of N beads and total length $L = l_0(N-1)$, where the position of bead i is $\mathbf{r}_i$. The scale bar is 5 μm.

$L = l_0(N-1)$ and persistence length l_p, as seen in Fig. 1; the chain parameters N, a, l_0, and l_p, as well as the input parameters f and H_0, can be measured and tuned experimentally. We implement a numerical model to verify our understanding of the forces present in the colloidal model and their subsequent effect on the dynamics. These Brownian dynamics simulations were carried out on the DAVinCI cluster at Rice University and the Stampede cluster at the Texas Advanced Computing Center.

We confine the chain to the x-y plane such that gravity has no influence. For the ith bead along the backbone of the chain, we can write the equation of motion

$$m_i \frac{d^2\mathbf{r}_i}{dt^2} = \mathbf{F}_i^{\text{chain}} + \mathbf{F}_i^{\text{magnetic}} + \mathbf{F}_i^{\text{hydro}} + \mathbf{F}_i^{\text{Brownian}}, \tag{1}$$

where $\mathbf{F}_i^{\text{chain}}$ is the extensional spring and bending forces governing the chain, $\mathbf{F}_i^{\text{magnetic}}$ accounts for forces due to the external field, $\mathbf{F}_i^{\text{hydro}}$ is the hydrodynamic drag force, and $\mathbf{F}_i^{\text{Brownian}}$ is a stochastic term accounting for thermal fluctuation; due to the magnitudes of our magnetic fields and velocities, we posit that the first three force terms drive the dynamics of this system and as such a simpler uncorrelated Brownian fluctuation is sufficient to capture the dynamics that we observe experimentally. Beads are numbered from $i = 1$ to N, with position $\mathbf{r}_i$, and between each bead we draw a connecting vector $\mathbf{t}_i = \mathbf{r}_i - \mathbf{r}_{i-1}$, which has magnitude $l_i = |\mathbf{t}_i|$.

At the low-Re limit, the beads have negligible inertial effects. An integration scheme to handle this scenario was proposed by Ermak and MacCammon [29], where the position of each bead i after a time Δt, $\mathbf{r}_i(t + \Delta t)$ is calculated from the current position $\mathbf{r}_i(t)$ by

$$\mathbf{r}_i(t + \Delta t) = \mathbf{r}_i(t) + \sum_j \frac{\mathbf{D}_{ij}(t)\mathbf{F}_j(t)}{k_b T}\Delta t + R_i(\Delta t), \tag{2}$$

where $\mathbf{D}_{ij}$ is the Rotne-Prager diffusion matrix, k_bT is the thermal energy, and $R_i(\Delta t)$ is a random displacement following a Gaussian distribution with zero mean and variance, covering the hydrodynamic and Brownian contributions. The remaining forces are encompassed by $\mathbf{F}_j(t)$, which is the sum of magnetic, bending, and stretching contributions between beads, i.e.,

$$\mathbf{F}_j = \mathbf{F}_j^{\text{spring}} + \mathbf{F}_j^{\text{bend}} + \mathbf{F}_j^{\text{magnetic}}. \tag{3}$$

The extensional force between beads is treated with a linear spring

$$\mathbf{F}_j^{\text{spring}} = -\nabla_j U^{\text{spring}} = -k[l_j - l_0]\hat{\mathbf{t}}_j + k[l_{j+1} - l_0]\hat{\mathbf{t}}_{j+1}, \tag{4}$$

where k is a linear spring constant, $\mathbf{t}_j$ is the center-to-center vector between bead $j-1$ and bead j, $l_j = |\mathbf{t}_j|$ is the distance between the two beads, and l_0 is the equilibrium distance between beads. To describe the bending energy of the chain, we use a discretized version of the bending force, where the energy is written as a function of the angle between any three adjacent beads $U^{\text{bend}} = \frac{A}{l_0}\sum_{j=1}^{N} f_j[1 - \hat{\mathbf{t}}_{j+1}\cdot\hat{\mathbf{t}}_j]$. The force is then [1]

$$\begin{aligned}\mathbf{F}_j^{\text{bend}} = \frac{A}{l_0}\Bigg(&\frac{f_{j-1}}{l_j}\hat{\mathbf{t}}_{j-1} - \left[\frac{f_{j-1}}{l_j}\hat{\mathbf{t}}_{j-1}\hat{\mathbf{t}}_j + \frac{f_j}{l_{j+1}} + \frac{f_j}{l_j}\hat{\mathbf{t}}_j\hat{\mathbf{t}}_{j+1}\right]\hat{\mathbf{t}}_j \\ &+ \left[\frac{f_j}{l_{j+1}}\hat{\mathbf{t}}_j\hat{\mathbf{t}}_{j+1} + \frac{f_j}{l_j} + \frac{f_{j+1}}{l_{j+1}}\hat{\mathbf{t}}_{j+1}\hat{\mathbf{t}}_{j+2}\right]\hat{\mathbf{t}}_{j+1} - \frac{f_{j+1}}{l_{j+1}}\hat{\mathbf{t}}_{j+2}\Bigg),\end{aligned} \tag{5}$$

$$f_j = \begin{cases} 1 & \text{for } 2 \leqslant j \leqslant N-1 \\ 0 & \text{for } 1, N. \end{cases} \tag{6}$$

Note that $A = k_b T l_p$ and as such we can input experimentally determined persistence lengths.

In addition to spring and bending forces, there are magnetic forces acting on the particles as well. Each colloidal particle is paramagnetic and as such acquires a dipole when subjected to an external field

$$\mathbf{m} = \tfrac{4}{3}\pi r^3 \chi \mathbf{H}_{\text{ext}}, \tag{7}$$

where χ is the magnetic susceptibility of the particle and $\mathbf{H}_{\text{ext}}$ is the externally applied field.

Using the simplest dipolar model [30], the resulting magnetic force between any two dipoles is

$$\mathbf{F}_j^{\text{magnetic}} = -\nabla_j U_j^{\text{magnetic}} = \frac{3|\mathbf{m}|^2}{4\pi\mu_0 r^4}[3\cos^2\theta - 1]\hat{\mathbf{t}} + \frac{3|\mathbf{m}|^2}{4\pi\mu_0 r^4}\sin(2\theta)\hat{\boldsymbol{\theta}}, \tag{8}$$

where θ is the angle between $\mathbf{t}_j$ and $\mathbf{H}_{\text{ext}}$, r is the distance between the particles, $\hat{\boldsymbol{\theta}}$ is the polar angle coordinate, and μ_0 is the permeability of free space. We approximate the cumulative magnetic force on a given bead by summing the magnetic force contribution on each pair of beads in the system.

Combined, we can calculate $\mathbf{F}_j$ at a given time step and use Eq. (2) to step our simulation forward in time, starting from an initial condition of a linear chain aligned along the x axis. A full description of the parameters used in the system can be found in Appendix A.

III. THEORY

The primary forces that govern the dynamics are the driving magnetic force, the hydrodynamic drag resisting the motion of each particle, and elastic forces due to the DNA linkers between adjacent beads, which act as a restorative force. Having defined the forces, we seek analytical predictions of the dynamics various rotational dynamics that we observe. To do so, we must understand the balance of forces on the chain, which we describe using two dimensionless numbers: the Mason number Ma and magnetoelastic number Mn.

A. Magnetic and viscous forces

When a chain is driven to rotate by an external magnetic field, the Mason number describes the relative magnitudes of the driving magnetic force and the counteracting viscous drag [31]

$$\text{Ma} = \frac{144\pi\eta f}{\mu_0 \chi^2 H_0^2}, \tag{9}$$

where η is the fluid viscosity, μ_0 is the vacuum permeability, and χ is the magnetic susceptibility of each particle. When the torques applied by these two forces are in balance, the chain rotates at a constant angular velocity synchronous with the period of the external field [19,31–33]. In order to overcome viscous drag, the chain may rotate with increasing phase lag θ from the external field, thus increasing the magnetic torque to balance. If more magnetic torque is required than is available, unlinked chains will fragment [32,33]. However, DNA-linked chains will instead deform to form metastable and collapsed structures [19].

The viscous torque on a chain of beads rotating about its center can be described by a shish-kebab model, i.e., a bead model that is locked into a linear configuration with $l_0 = d$ [34],

$$\Gamma_v = \frac{8\pi b a^3 N^3 \eta \omega}{3 \ln\left(\frac{N}{2}\right)}. \tag{10}$$

Here b scales the viscous torque, as it drops rapidly with increased bead spacing [1], from a value of $b = 1$ for a shish kebab ($l_0 = d$), dropping to about $b = 0.36$ for our measured values of $l_0 \approx 1.3d$ [35].

For a pair of point dipoles, the magnetic force can be approximated by taking Eq. (8) with $r = 2a$. Under the assumption of a linear chain at constant lag angle θ from the external field, each pair of dipoles has magnetic forces that cancel out exactly [20,33] such that only the first and last beads, with a single neighbor each, have nonzero net forces. The torque is then simple to calculate

$$\Gamma_m = 2F_\theta[2ai]_{i=N/2} = \frac{12\pi a^3 N \eta \omega}{\mathrm{Ma}} \sin 2\theta. \tag{11}$$

Balancing this magnetic torque with the viscous torque, using the maximum magnetic torque at $\sin 2\theta = 1$, we find

$$\mathrm{Ma}_c = \frac{9}{2} \frac{\ln\left(\frac{N}{2}\right)}{bN^2}. \tag{12}$$

Below this critical curve, torques can be balanced and rigid rotation achieved. Above the curve, a balance cannot be achieved even with a maximum phase lag of $\theta = \pi/2$.

B. Magnetic and elastic forces

In between synchronous rotation and rotational equilibrium we see a rich dynamical regime: Magnetic, viscous, and elastic forces all compete as a chain undergoes asynchronous rotation. To identify the critical values of Ma and Mn at which these behaviors occur, we calculate torque balances on the chain.

In this deformation regime, we use the critical values of Mn to predict the specific behavior. These critical values correspond to buckling instabilities: For example, the first mode ($n = 1$) corresponds to a hairpin, the second mode ($n = 2$) to an S curve, etc. [36].

If a chain is in stationary rotational equilibrium, the magnetic force has radial components that are resisted by the elasticity of the chain. The magnetoelastic number describes the relative magnitude of these two forces [37], i.e.,

$$\mathrm{Mn} = \frac{\pi \mu_0 a^2 H_0^2 L^2}{6A} \frac{\chi^2/4}{(1 - \chi/6)(1 + \chi/12)}. \tag{13}$$

This dimensionless group is used to predict the buckling instabilities that result from the competing magnetic and elastic forces; critical values of the buckling instability can be calculated to be

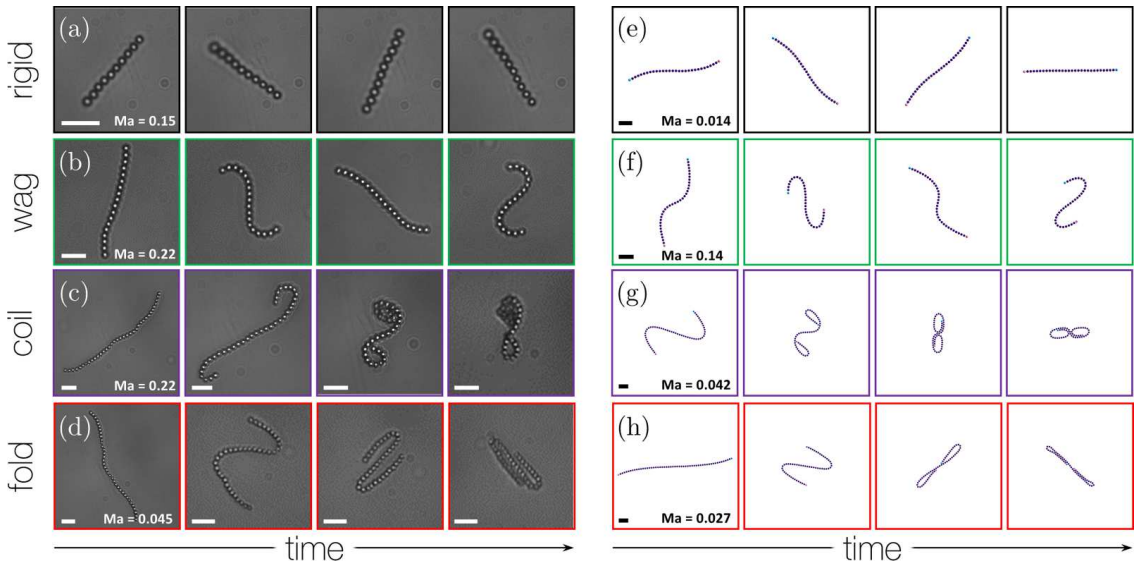

FIG. 2. Snapshots at selected times of (a)–(d) experimental and (e)–(h) numerical examples of rigid rotators, wagging chains, coiling chains, and folded chains in the course of their dynamics. In each series, the magnetic field is rotating counterclockwise across time and all scale bars are 5 μm. The magnetic field is rotating with f from 0.1 to 1 Hz, with H_0 varying from 39 G to 70 G. See [42] for videos of the various rotational regimes.

$\mathrm{Mn}_c = (2n\pi)^2$, as derived in Appendix B, corresponding to increasing numbers of bending modes [2,37–41].

We are interested in the eigenvalue for $n = 2$, as this mode corresponds to the stability of an S curve:

$$\mathrm{Mn}_c = (2n\pi)^2 = 16\pi^2. \tag{14}$$

We then substitute Eq. (13) into Eq. (9), yielding

$$\mathrm{Ma}_s = \frac{1}{\mathrm{Mn}_c} \frac{24\pi^2 \eta f a^4 N^2}{A(1-\chi/6)(1+\chi/12)}, \tag{15}$$

above which the S curve is stable and below which higher modes of buckling instability should take precedence.

IV. RESULTS AND DISCUSSION

Throughout the course of our experiments and simulations, we find that despite the persistence length being kept constant, four distinct rotational modes are observed: rigid rotation, wagging, coiling, and folding. For rigid rotation, the semiflexible chains maintain a close to linear conformation and rotate at a constant angular velocity, synchronous with the rotation of the external field, as can be seen in Fig. 2. In this mode, the chain has minimal bending energy and behaves as expected for an object in perfect rotational equilibrium.

As the driving forces compete to balance with the hydrodynamic drag, the chain may rotate asynchronously with the external field, leading to new, nonrigid rotational modes. In one that we term wagging, the two tail ends will periodically wag back and forth with a beating frequency that appears to be uncorrelated with the angular motion. The tail ends deform in the direction of rotation while the center of the chain is relatively stationary; afterward, the center of the chain rotates as the tail ends relax, resulting in a time-dependent bending energy. There is some evidence that this mode is unstable and sensitive to perturbations.

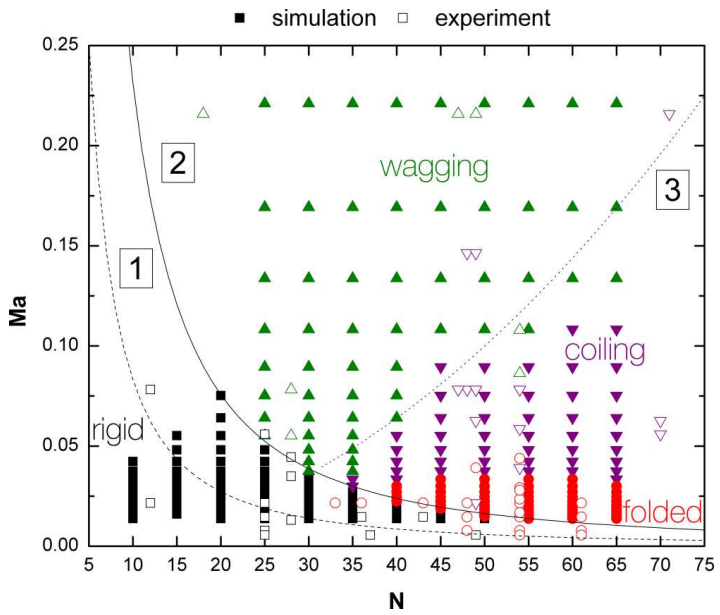

FIG. 3. State diagram of rotational regimes as the chain length and driving magnetic field is varied. Rigid (black ■), wagging (green ▲), coiling (purple ▼), and folded (red ●) chains are observed in both simulation (closed symbols) and experiment (open symbols). The theoretical balances on the limits of rigid rotation [1] [Eq. (12)] shifts to [2] when $b = 0.36$. The expected stability of S curves [3] [Eq. (15)] is also shown for $f = 0.1$, falling between the wagging and coiling regimes.

Additional dynamics are observed with increasing N, such as coiling events that are comparable to those seen in the literature [9,10,19]. The initial dynamics appear similar to the first beat of a wagging period, but instead of relaxing at the end of the beat, the tails fold over to deform further. The second fold leads to the chain coiling on itself and appears to eventually reach a state of rigid rotation, albeit in a more compact, lower drag configuration.

Longer chains can fold upon themselves to reduce the drag on the chain. After folding, the chain has several linear lengths, which align roughly parallel to each other. The folded configuration then behaves as a rigid rotator of a shortened length.

We combine our experimental, numerical, and analytical results in a state diagram, as shown in Fig. 3, where the choice of axes compares the input force parameters, as encompassed by the Mason number, with the length of the chain N, the chain parameter being varied. When plotted according to their dynamics, we see that the four behaviors (rigid, wagging, coiling, and folding) separate into distinct regimes, with remarkable agreement between experimental and computational results.

First, we note that Eq. (12) with $b = 1$ appears to underestimate the actual limit of the rigid rotator regime by a factor of about 2.5. This is corrected when the bead spacing l_0 is accounted for, indicating that the differences in drag between the analytical shish-kebab model and real bead-spring models are non-negligible.

Below this curve is the low-Ma regime, where the magnetic torque is large enough to dominate, leading to rigid rotation. In this context, we can interpret the existence of folded rotators, where the magnetic torque is not large enough to overcome the viscous drag. By folding, the chains effectively lower N and, by extension, its viscous drag, maintaining a constant Ma until they enter the rigid regime.

Above this curve, the viscous and elastic forces compete with the magnetic force, resulting in more complicated dynamics. We then plot the balance predicting buckling instabilities. Equation (15) with $n = 2$ successfully demarcates wagging and coiling behavior, which is indeed the transition from an S curve to higher-mode buckling. Increasing n further lowers the curve, which is consistent with the location of the high-mode coiling regime on this diagram.

V. CONCLUSION

In this work, we have demonstrated the application of colloidal chains to study the effect of flexibility on filament dynamics in a steadily rotating magnetic force field. We have identified parameter ranges that can yield both expected dynamics, such as steady rigid rotation, as well as new dynamics, in the reversibly deforming wagging region. Through simple physical arguments, we are able to predict the parameter space in which each dynamical regime should reside.

There are a number of questions still to be addressed. For example, we experimentally observe asymmetrical coiling behaviors that we cannot predict with our torque balances, but which are certainly useful to harness for practical application [22]. We have also observed chains move between wagging and coiling before settling, which suggests that some rotational regimes may be metastable and sensitive to perturbation. In particular, there is some overlap in Fig. 3 between the wagging and coiling regimes, which may be indicative of state transitions or coexistence and warrants further study. Finally, the beating frequency of the wagging modes, and whether it has a regular cycle of competing forces or falls into chaotic behavior, is still an open question, and a firm grasp of the dynamics is critical to development of artificial cilia and other microswimmers.

In summary, we have demonstrated the use of a colloidal chain model and its application in identifying and predicting the detailed rotational dynamics of semiflexible filaments at backbone-level subperiod resolution. We found that our colloidal particle chain compares favorably with a computational bead-spring model and that its resemblance to theoretical models allows us to analytically predict the rotational dynamics knowing the applied external force and the length of the chain. With such a controllable experimental model at our disposal, we can begin to explore force regimes where simulations become prohibitively costly, such as at high N or with multiple fiber interactions, where such detailed resolution has implications ranging from the complicated topology of a single self-entangled fiber to the origin of bulk properties of more concentrated solutions.

ACKNOWLEDGMENTS

This work was supported in part by the National Science Foundation under Grant No. CBET-1705703 and the Data Analysis and Visualization Cyberinfrastructure funded by NSF under Grant No. OCI-0959097 and Rice University. This work also used the Extreme Science and Engineering Discovery Environment, which is supported by National Science Foundation Grant No. ACI-1548562. The authors acknowledge the Texas Advanced Computing Center at University of Texas at Austin for providing high performance computing resources that have contributed to the research results reported within this paper.

APPENDIX A: SIMULATION PARAMETERS

A summary of our experimental and simulation parameters is given in Table I. Note that the experimental parameters are measured from experiment and the simulation parameters are inputs, with the exception of the spring constant k, which is set high with an appropriately small Δt to approximate an inextensible fiber.

APPENDIX B: STABILITY OF AN S CURVE

In Ref. [37], the authors derive the inextensibility and equations of motion for a viscous and elastic filament. For small, steady deformations away from orthogonality to the field, the system is linearized to

$$0 = -\frac{\partial^4 \theta}{\partial s^4} - \mathrm{Mn}\frac{\partial^2 \theta}{\partial s} \tag{B1}$$

TABLE I. Summary of experimental and simulation parameters in Secs. II A and II B.

Parameter	Experiment	Simulation
N	5–75	5–75
a	0.535 μm	0.535 μm
l_0	1.4 μm	1.366 μm
l_p	1.3 mm	1.325 mm
T	298 K	298.15 K
η	0.0022 kg/m s	0.0022 kg/m s
χ	1.377	1.377
ω	0.1–1 Hz	0.1–1 Hz
H_0	10–70 G	10–70 G
Δt		2.0×10^{-6} s
k		12000 N/m

with boundary conditions

$$\left.\frac{\partial\theta}{\partial s}\right|_{s=\pm 1/2} = \left.\frac{\partial^2\theta}{\partial s^2} + \mathrm{Mn}\theta\right|_{s=\pm 1/2} = 0 \tag{B2}$$

for free ends and

$$\left.\theta\right|_{s=0} = \left.\frac{\partial\theta}{\partial s}\right|_{s=0} = 0 \tag{B3}$$

for a reference frame pinned to rotate about the center. The solution yields the eigenvalues

$$\sqrt{\mathrm{Mn}}\tfrac{1}{2} = n\pi \tag{B4}$$

for the modes. We are interested in the mode $n = 2$, as this corresponds to the stability of an S curve:

$$\mathrm{Mn}_c = (2n\pi)^2 = 16\pi^2. \tag{B5}$$

[1] E. Gauger and H. Stark, Numerical study of a microscopic artificial swimmer, Phys. Rev. E **74**, 021907 (2006).

[2] R. Dreyfus, J. Baudry, M. Roper, M. Fermigier, H. Stone, and J. Bibette, Microscopic artificial swimmers, Nature (London) **437**, 862 (2005).

[3] S. Camalet, F. Jülicher, and J. Prost, Self-Organized Beating and Swimming of Internally Driven Filaments, Phys. Rev. Lett. **82**, 1590 (1999).

[4] S. Biswal and A. Gast, Micromixing with linked chains of paramagnetic particles, Anal. Chem. **76**, 6448 (2004).

[5] M. Vilfan, A. Potočnik, B. Kavčič, N. Osterman, I. Poberaj, A. Vilfan, and D. Babič, Self-assembled artificial cilia, Proc. Nat. Acad. Sci. U.S.A. **107**, 1844 (2010).

[6] C. Huang, G. Gompper, and R. Winkler, Non-equilibrium relaxation and tumbling times of polymers in semidilute solution, J. Phys.: Condens. Matter **24**, 284131 (2012).

[7] I. Kirchenbuechler, D. Guu, N. Kurniawan, G. Koenderink, and M. Lettinga, Direct visualization of flow-induced conformational transitions of single actin filaments in entangled solutions, Nat. Commun. **5**, 5060 (2014).

[8] G. B. Jeffery, The motion of ellipsoidal particles immersed in a viscous fluid, Proc. R. Soc. London Ser. A **102**, 161 (1922).
[9] O. L. Forgacs and S. G. Mason, Particle motions in sheared suspensions: IX. Spin and deformation of threadlike particles, J. Colloid Sci. **14**, 457 (1959).
[10] O. L. Forgacs and S. G. Mason, Particle motions in sheared suspensions: X. Orbits of flexible threadlike particles, J. Colloid Sci. **14**, 473 (1959).
[11] D. Smith, H. Babcock, and S. Chu, Single-polymer dynamics in steady shear flow, Science **283**, 1724 (1999).
[12] P. LeDuc, C. Haber, G. Bao, and D. Wirtz, Dynamics of individual flexible polymers in a shear flow, Nature (London) **399**, 564 (1999).
[13] R. Teixeira, H. Babcock, E. Shaqfeh, and S. Chu, Shear thinning and tumbling dynamics of single polymers in the flow-gradient plane, Macromolecules **38**, 581 (2005).
[14] P. Skjetne, R. Ross, and D. Klingenberg, Simulation of single fiber dynamics, J. Chem. Phys. **107**, 2108 (1997).
[15] C. G. Joung, N. Phan-Thien, and X. J. Fan, Direct simulation of flexible fibers, J. Non-Newton. Fluid **99**, 1 (2001).
[16] H. Kobayashi and R. Yamamoto, Tumbling motion of a single chain in shear flow: A crossover from Brownian to non-Brownian behavior, Phys. Rev. E **81**, 041807 (2010).
[17] P. S. Lang, B. Obermayer, and E. Frey, Dynamics of a semiflexible polymer or polymer ring in shear flow, Phys. Rev. E **89**, 022606 (2014).
[18] S. Liu, B. Ashok, and M. Muthukumar, Brownian dynamics simulations of bead-rod-chain in simple shear flow and elongational flow, Polymer **45**, 1383 (2004).
[19] S. L. Biswal and A. P. Gast, Rotational dynamics of semiflexible paramagnetic particle chains, Phys. Rev. E **69**, 041406 (2004).
[20] I. Petousis, E. Homburg, R. Derks, and A. Dietzel, Transient behavior of magnetic micro-bead chains rotating in a fluid by external fields, Lab Chip **7**, 1746 (2007).
[21] N. Coq, S. Ngo, O. du Roure, M. Fermigier, and D. Bartolo, Three-dimensional beating of magnetic microrods, Phys. Rev. E **82**, 041503 (2010).
[22] T. Yang, T. O. Tasci, K. B. Neeves, N. Wu, and D. W. M. Marr, Magnetic microlassos for reversible cargo capture, transport, and release, Langmuir **33**, 5932 (2017).
[23] E. J. Hinch and L. G. Leal, The effect of Brownian motion on the rheological properties of a suspension of non-spherical particles, J. Fluid Mech. **52**, 683 (1972).
[24] C. M. Schroeder, R. E. Teixeira, E. S. G. Shaqfeh, and S. Chu, Characteristic Periodic Motion of Polymers in Shear Flow, Phys. Rev. Lett. **95**, 018301 (2005).
[25] M. Harasim, B. Wunderlich, O. Peleg, M. Kröger, and A. R. Bausch, Direct Observation of the Dynamics of Semiflexible Polymers in Shear Flow, Phys. Rev. Lett. **110**, 108302 (2013).
[26] G. Fonnum, C. Johansson, A. Molteberg, S. Mørup, and E. Aksnes, Characterisation of Dynabeads® by magnetization measurements and Mössbauer spectroscopy, J. Magn. Magn. Mater. **293**, 41 (2005).
[27] J. Byrom, P. Han, M. Savory, and S. Biswal, Directing assembly of DNA-coated colloids with magnetic fields to generate rigid, semiflexible, and flexible chains, Langmuir **30**, 9045 (2014).
[28] J. C. Crocker and E. R. Weeks, Particle tracking using IDL, http://www.physics.emory.edu/faculty/weeks//idl/
[29] D. Ermak and J. McCammon, Brownian dynamics with hydrodynamic interactions, J. Chem. Phys. **69**, 1352 (1978).
[30] M. Fermigier and A. P. Gast, Structure evolution in a paramagnetic latex suspension, J. Colloid Interface Sci. **154**, 522 (1992).
[31] D. Du, E. Hilou, and S. L. Biswal, Modified Mason number for charged paramagnetic colloidal suspensions, Phys. Rev. E **93**, 062603 (2016).
[32] S. Melle and J. Martin, Chain model of a magnetorheological suspension in a rotating field, J. Chem. Phys. **118**, 9875 (2003).
[33] Y. Gao, M. A. Hulsen, T. G. Kang, and J. M. J. den Toonder, Numerical and experimental study of a rotating magnetic particle chain in a viscous fluid, Phys. Rev. E **86**, 041503 (2012).

[34] M. Doi and S. F. Edwards, *The Theory of Polymer Dynamics* (Clarendon, Oxford, 1988).
[35] B. Cichocki, B. Felderhof, K. Hinsen, E. Wajnryb, and J. Blawzdziewicz, Friction and mobility of many spheres in Stokes flow, J. Chem. Phys. **100**, 3780 (1994).
[36] A. Cebers, Flexible magnetic filaments, Curr. Opin. Colloid Interface Sci. **10**, 167 (2005).
[37] M. Roper, R. Dreyfus, J. Baudry, M. Fermigier, J. Bibette, and H. Stone, On the dynamics of magnetically driven elastic filaments, J. Fluid Mech. **554**, 167 (2006).
[38] A. Cebers, Dynamics of a chain of magnetic particles connected with elastic linkers, J. Phys.: Condens. Mat. **15**, S1335 (2003).
[39] A. Cebers, Dynamics of elongated magnetic droplets and elastic rods in magnetic field, J. Magn. Magn. Mater. **289**, 335 (2005).
[40] A. Cebers and K. Erglis, Flexible magnetic filaments and their applications, Adv. Funct. Mater. **26**, 3783 (2016).
[41] M. Roper, R. Dreyfus, J. Baudry, M. Fermigier, J. Bibette, and H. Stone, Do magnetic micro-swimmers move like eukaryotic cells? Proc. R. Soc. London Ser. A **464**, 877 (2008).
[42] See Supplemental Material at http://link.aps.org/supplemental/10.1103/PhysRevFluids.2.104102 for movies corresponding to the images in Fig. 2.